AIP Advances

Series arrays of planar long Josephson junctions for high dynamic range magnetic flux detection

Cite as: AIP Advances **9**, 105215 (2019); https://doi.org/10.1063/1.5126035
Submitted: 28 August 2019 . Accepted: 04 October 2019 . Published Online: 18 October 2019

Jay C. LeFebvre, Ethan Cho, Hao Li, Kevin Pratt, and Shane A. Cybart

Series arrays of planar long Josephson junctions for high dynamic range magnetic flux detection

Cite as: AIP Advances 9, 105215 (2019); doi: 10.1063/1.5126035
Submitted: 28 August 2019 • Accepted: 4 October 2019 •
Published Online: 18 October 2019

Jay C. LeFebvre,[1] Ethan Cho,[2] Hao Li,[2] Kevin Pratt,[3] and Shane A. Cybart[2,4,a)]

AFFILIATIONS

[1]Department of Physics and Astronomy, University of California Riverside, Riverside, California 92507, USA
[2]Department of Electrical and Computer Engineering, University of California Riverside, Riverside, California 92507, USA
[3]Tristan Technologies, Inc., San Diego, California 92121, USA
[4]Materials Science and Engineering, University of California Riverside, Riverside, California 92507, USA

[a)]Electronic mail: cybart@ucr.edu

ABSTRACT

We investigated series arrays of closely spaced, planar long Josephson junctions for magnetic field transduction in Earth's field, with a linear response and high dynamic range. The devices were fabricated from thin film high-temperature superconductor $YBa_2Cu_3O_{7-\delta}$ (YBCO) thin films, using focused helium ion beam irradiation to create the Josephson barriers. Four series arrays, each consisting of several hundreds of long junctions, were fabricated and electrically tested. From fits of the current-voltage characteristics, we estimate the standard deviation in critical current to be around 25%. Voltage-magnetic field measurements exhibit a transfer function of 42 mV/mT and a linear response over a range of 303 μT at 71 K, resulting in a dynamic range of 124 dB.

Josephson junction devices are a leading candidate for magnetic field sensing due to their unique capability to quantum mechanically transduce magnetic flux into voltage. The most mature Josephson-based technology for sensing applications is the DC superconducting quantum interference device (SQUID). SQUID based systems are arguably the most sensitive magnetometers and have long been used in a diverse range of applications for detection.[1,2] Unfortunately, SQUIDs have limitations in bandwidth and upper operation frequency that complicate sensing above 100 MHz. The limitations are not intrinsic to the SQUID itself but rather the flux-locked-loop readout electronics used to linearize the output voltage of the SQUID.

Successful efforts have been made operating SQUID sensors without feedback electronics, termed "unlocked" operation. However, this comes at the expense of dynamic range and linearity. A great deal of research has been performed to improve unlocked operation by utilizing arrays of small area SQUIDs connected either in series, parallel, or a combination of both.[3–6] The benefits of a parallel SQUID array are reduced constraints on junction uniformity and increased effective area at the cost of decreased voltage response. Sensitivity, defined by the device transfer function, may be maintained through increasing the sensor voltage response by connecting very large numbers of SQUIDs together in series with the detriment to increased noise and strict junction uniformity requirements. SQUID arrays have demonstrated improvement in bandwidth and dynamic range, yet better linearity of the voltage response is still desired. Approaches to engineer the array geometry to produce a more linear voltage response yielded some improvement.[7] However, the intrinsic non-linearity of the SQUID transfer function and the susceptibility of the SQUID loop inductances to small temperature changes make this approach very difficult.[8]

An alternative approach to unlocked superconducting high-linearity, wide-bandwidth, high-dynamic range magnetic field sensors is single Josephson junctions.[9] Single Josephson junctions have the benefits of reducing geometrical inductances, flux noise, and size, but comes at the cost of decreased sensitivity. To improve single junction sensitivity, we propose to utilize long Josephson junctions. Long junctions are defined by having a geometric dimension parallel to the barrier interface (w) being greater than the Josephson

penetration depth (λ_J). Long junctions increase the coupling to an applied magnetic flux by increasing the area of the junction, and have been used in several other Josephson devices.[10,11]

In Josephson junctions the critical current (I_C) modulates as a function of magnetic flux penetrating the junction. The modulus of the Fourier transform of the current distribution in the junction yields the maximum current density.[12] In the short junction regime ($w < \lambda_J$), the current is uniformly distributed and the Fourier transform results in the familiar Fraunhofer diffraction pattern: $I_C(\Phi) = I_C(0)|sin(\Phi/\Phi_0)/(\Phi/\Phi_0)|$. Where Φ is the magnetic flux threading the junction, and Φ_0 is the magnetic flux quanta. In contrast, in the long junction regime ($w > \lambda_J$), the current is screened from the center of the junction and the resulting I_C modulation results in a sharper zero-bias peak and a shorter diffraction period.[13–15] Additionally, a self-field penetrates long Josephson junctions generated by the current in the superconducting electrodes which skews the main peak away from zero applied magnetic field in the maximum current response.[16,17] These effects have been well documented in low temperature superconducting Josephson junctions.[18]

In comparison to a SQUID, this periodicity in flux is typically orders of magnitude larger because the area of the junction is much smaller than the loop of the SQUID. As a result, Josephson junction magnetic field sensors have the potential to operate in unshielded environments with a large background magnetic field. Unfortunately, the increase in dynamic range comes at the expense of decreased sensitivity. This may be mitigated by connecting large numbers of junctions in a series array to increase the signal, because in these devices the amplitude of the voltage modulation scales proportionally to the number of junctions.[19,20] Parallel arrays can also dramatically increase sensitivity; however, interference effects between junctions in parallel result in a highly nonlinear voltage response to applied magnetic flux which would be undesirable for unlocked operation. We want to utilize the natural linear response of long Josephson junctions in series arrays for high dynamic range, wide bandwidth magnetic field sensors.

For fabrication of a large number of Josephson junctions in series we take advantage of a property of cuprate superconductors. Ion irradiation causes disorder in the cuprate $YBa_2Cu_3O_{7-\delta}$ (YBCO) that lowers the critical temperature and causes it to transition from a conductor to an insulator and has been shown to be suitable for fabrication of Josephson junctions.[21–23] YBCO is chosen for its high sensitivity to disorder and for having a critical temperature above the boiling point of nitrogen. In this work, we examine series arrays of long Josephson junctions in YBCO thin films with a planar geometry fabricated using helium ion irradiation from a focused helium ion microscope (FHIM).[24,25] Fig. 1 represents the FHIM irradiating a YBCO electrode and depicts the planar geometry of a single Josephson junction. This method of ion irradiation allows for the maskless nanoscale fabrication of interfaceless junctions with variable parameters, removing constraints on positioning, and lending itself for large scale fabrication of junction arrays.

Planar Josephson junction geometry offers an advantage for magnetic field sensing due to flux focusing effects. In the planar geometry, Meissner screening leads to a spreading of the magnetic field lines along the surface resulting in a focusing effect at the Josephson barrier, with the consequence of enhancing sensitivity.[11]

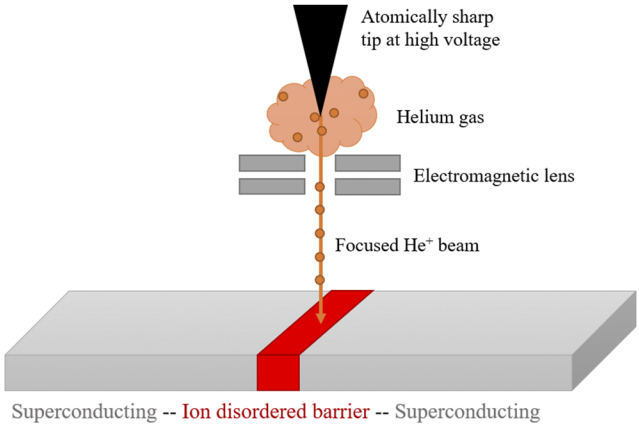

FIG. 1. Representation of the Zeiss Orion Plus focused helium ion microscope consisting of an atomically sharp tip maintained at a high voltage. When helium gas is introduced to the tip electric field the helium is ionized and accelerated through a series of electromagnetic lenses to focus and control the beam to a nanoscale spot size. Allowing precise ion irradiation of thin film YBCO (gray) to fabricate Josephson junctions in a planar geometry.

Sensitivity is proportional to the I_C magnetic modulation period (ΔB). For planar junctions with an electrode width greater than the length, $\Delta B = 1.842\Phi_0/w^2$.[26] Much research has been done to understand the behavior of planar long Josephson junctions and is now well understood.[27,28]

We investigated connecting hundreds of FHIM irradiated planar long Josephson junctions into a series array for magnetic field sensing. For fabrication of our device we begin with 32-nm films of YBCO on LSAT substrates capped with a 200-nm thick layer of gold. These films were purchased from Ceraco GmBH and grown with reactive co-evaporation.[29] On four separate samples 2.5 mm long superconducting electrodes with electrode widths 10 and 20 μm were patterned with conventional photolithography and argon ion milling. The gold layer was removed with a KI^+ chemical etch to uncover the YBCO electrodes to ensure that He^+ ion irradiation can fully penetrate the film and create a uniform disordered region. Samples were loaded into a FHIM and junction barriers were written using a 0.5 nm, 36 keV, 0.5 pA helium ion beam.

The device geometry can be viewed in Fig. 2. Fig. 2(b) provides an expanded view, making visible three parallel electrodes. The middle electrode consists of YBCO with the gold cap removed and contains the long junction array. The two adjacent electrodes are magnetic control lines consisting of gold capped YBCO. Also, indicated on Fig. 2(b) are the locations of the Josephson junctions, as indicated by red lines. The red lines are not to scale and only indicate the junction positions. The actual junction barrier is only a few nanometers. Note that the YBCO is highly sensitive to the disorder caused by the irradiation, and therefore, the dose required for writing junctions is orders of magnitude less than that required for milling or removing material. Consequently, the junctions are not able to be optically imaged after being written because the irradiated regions are optically indistinguishable from non-irradiated regions.

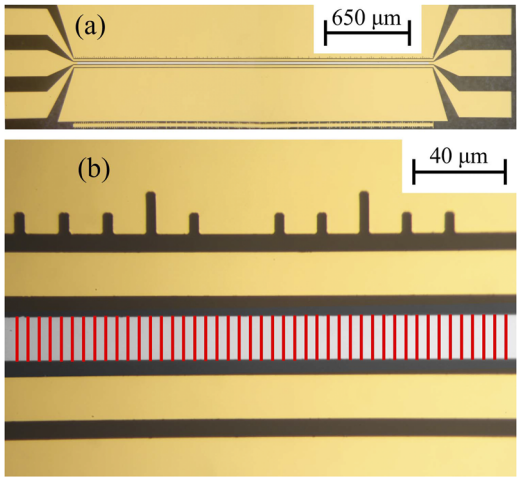

FIG. 2. (a) Image of the long junction array transducer. It consists of a central long junction array flanked by two on-chip control lines for flux biasing. (b) A detailed view of the array and control lines. The array has had the gold cap layer removed via chemical etching to open the YBCO for ion irradiation. The red lines represent the irradiated lines that define the Josephson barriers of the junctions. Tick marks near electrodes were used for FHIM alignment.

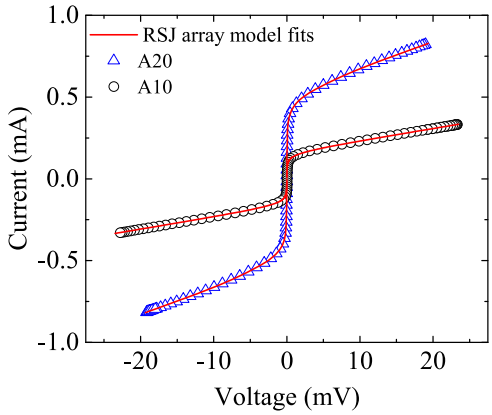

FIG. 3. Current-voltage characteristics of each device A10 (circle) and A20 (triangle). With an RSJ array model fit (red line) overlaid for each respective array width and was used to estimate the I_C deviation.

The parameter space for long junction array fabrication is expansive. Specific device properties and unique device identifiers are presented in Table I. Parameters such as junction width (w), number of junctions (N), junction irradiation dose, and interjunction spacing (Δ) were varied in each device for better understanding of optimization. Junctions were written with a FHIM by irradiating a line which crosses the entirety of the junction dimension perpendicular to the superconducting electrode. The junction barrier strength is proportional to the total number of ions per unit area and is termed "dose". The distance between each adjacent junction (Δ) was decided to ensure that it was greater than two times the Pearl length, the effective penetration depth of magnetic field in superconducting thin films. Furthermore, Δ was varied between samples to investigate changes in inductive coupling due to flux focusing effects.

For characterization of samples A10 and A20, the samples were mounted on a cold head prototype Aisin pulse tube cooler (2.5 W at 77 K). This cooler was preferred over the more common Sterling cooler to reduce the associated noise. This also allows measurements to be made in unshielded environments desirable in application settings.

Fig. 3 presents the current-voltage characteristics of each of the 600-junction arrays at 77 K. These characteristics were measured at 1 Hz with 1 kHz low pass filters. Overlaid on the data in Fig. 3 are the results of a resistively-shunted junction array model fit to the data. The fitting function consisted of the summation of 600 individual characteristics:

$$V = R\sum_{k=1}^{N}\sqrt{I^2 - I_{Ck}^2} \tag{1}$$

where R is array normal state resistance, V is voltage, I is bias current, and I_{Ck} is a set of fitting parameters which we used to estimate the deviation in junction parameters.[30] The model suggests there is a 26% and 23% deviation in I_C parameters respectively for devices A10 and A20. We believe these deviations are overestimated and only place a maximum limit on the spread in parameters because our model ignores the effects of excess current and thermal rounding on the current-voltage characteristic. From the fitting parameters for device A10 the mean critical current, 198 μA, and normal resistance, 91 Ω, product was measured to be 18 mV. From the fitting parameters for device A20 the mean critical current, 597 μA, and normal resistance, 37 Ω, product was measured to be 22 mV.

TABLE I. Device specific long junction array characteristics as measured at 77 K. In text specific arrays are referred to by their device identifier. Δ is the interjunction spacing, N is the number of junctions, Mean I_C is the mean value of fitted parameters I_{Ck}, R is the array normal state resistance, S is the sensitivity, and O is the operating range.

Device identifier	w (μm)	Dose[a] (ions/cm^2)	Δ (μm)	N	Mean I_C (μA) (Deviation)	R (Ω)	S (mV/mT)	O (μT)
A10	10	4×10^{16}	2	600	198 (26%)	91	8.4	330
A20	20	4×10^{16}	2	600	597 (23%)	37	8.5	240
B350	20	7×10^{16}	5	400	269 (26%)	12	16.7	146
B400	20	8×10^{16}	5	400	158 (41%)[b]	16	24	199

[a]Devices A* were fabricated on a Zeiss NanoFab, and devices B* were fabricated on a Zeiss Orion Plus.
[b]This number appears to be a gross overestimation by our fitting procedure likely due to the small I_C of this device.

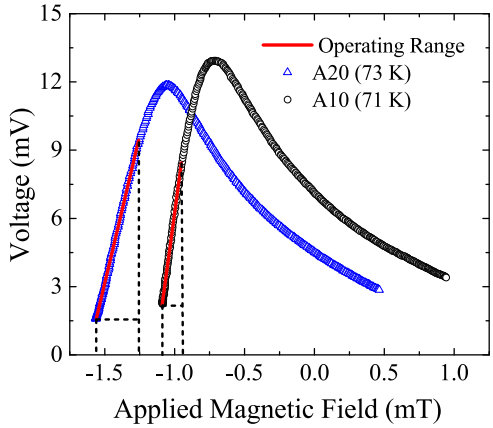

FIG. 4. Voltage-magnetic field characteristics for devices A10 (blue triangle) and A20 (black circle) at 71 and 73 K. A red line is overlaid on each magnetic modulation voltage response indicating the linear fit over the operating range of each device, while the black dotted lines aid the determination of the operating range.

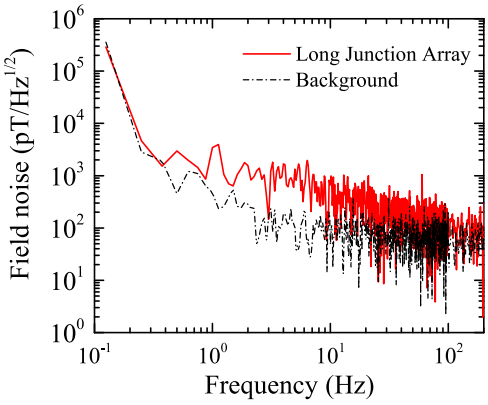

FIG. 5. Flux Signal noise spectrum of device B350 at 77 K (solid red) plotted alongside the background noise (dotted black).

The voltage-magnetic field measurements were made by DC current biasing the array just above the critical currents of the junctions and sweeping the magnetic field at 1 Hz. Fig. 4 yields the results at for arrays A10 and A20. An operating range (O) was determined by maximizing the range over which the Pearson's correlation value was greater than .999. This fit is plotted in the operating range as a visual aid in Fig. 4. Note the high operating range of 303 μT in the A20 array at 73 K, which is much greater than the Earth's magnetic field and is essential for unshielded operation. The sensitivity (S) was estimated from the slope of a linear fitting regime in the region of the operating range. The transfer function for the A10 array improved from 8.4 mV/mT at 77 K to 42 mV/mT as temperature is lowered to 71 K. Similarly, the transfer function for the A20 array improved from 8.5 mV/mT at 77 K to 26 mV/mT at 73 K. This is likely due to the increase of I_CR as the gap continues to open as well as from additional skewing from a decreasing Josephson penetration depth as the temperature is lowered.

As previously mentioned, these measurements were made without magnetic shielding. Effects of flux trapping were examined by performing multiple thermal cycles above T_C to expel trapped flux and subsequently cooled slowly to measurement temperatures and comparing the voltage modulation response to applied magnetic field. No significant changes to the magnetic field characteristics were observed between thermal cycles. We attribute the shift of the peak off of the applied field zero bias to residual fields and self-field effects.

Characterization of devices B350 and B400 were performed in a similar manner as A10 and A20 with the only significant difference being that the B* devices were cooled using a cryogenic dip probe, which also had no magnetic shielding. The characterization of the devices is summarized in Table I. A notable improvement in sensitivity in B* over A* devices is observed and is attributed to improved flux focusing effects by increasing the interjunction spacing.

Field noise is plotted in Fig. 5 for device B350 at 77 K. The noise was measured in an unlocked setup made by using batteries to current bias the junction above I_C and magnetically bias the device within the operating range with the magnetic control lines. The output was amplified by a Stanford Research Systems SR560 and input into a Hewlett Packard 3562A signal analyzer for measurement of the voltage noise. The device noise is plotted alongside the background preamplifier noise for comparison.

For B350 the field noise was measured to be 572 pT/Hz$^{1/2}$ at 10 Hz and 95 pT/Hz$^{1/2}$ at 100 Hz. B400 was measured similarly and the field noise was measured to be 368 pT/Hz$^{1/2}$ at 10 Hz and 202 pT/Hz$^{1/2}$ at 100 Hz. With the figures of merit noise and operating range we can define a dynamic range for the devices:

$$Dynamic\ Range = 20Log_{10}[OperatingRange/Noise] \quad (2)$$

For B350 we estimate a dynamic range of 108 dB at 10 Hz and 124 dB at 100 Hz, and for B400 we estimate 115 dB at 10 Hz and 120 dB at 100 Hz.

Series arrays of several hundred long junctions were fabricated to demonstrate their operating potential as magnetometers. A sensitivity of 42 mV/mT was achieved in a 10 μm long junction array with an operating range of 135 μT at 71 K promising a competitive performance for superconducting electronics. More investigation is suggested to establish proper scaling laws for the response in terms of the gain, noise, single tone dynamic range, and spur free dynamic range. We suggest that further optimization of junction and array parameters will allow for increased performance.

Furthermore, junction arrays are promising candidates for superconducting electronics because they can be designed to match impedance for a wide range of interface electronics. Additionally, the magnetic sensitivity of the long junction array scales proportionally with number of junctions in the array, suggesting arrays of thousands of junctions can achieve a very high sensitivity. If a long junction array's transfer function can be improved then they may become desirable due to high linearity, high dynamic range, as well as being robust against parameter spread which degrades performance.

This work was supported by AFOSR FA 9550-17-C-0006, FA 9550-15-1-0218, ARO Grant W911NF1710504 and NSF Grant No. 1664446.

REFERENCES

[1] J. Clarke and A. I. Braginski, *The SQUID handbook*, Vol. 1 (Wiley Online Library, 2004).

[2] H. Weinstock, *SQUID sensors: Fundamentals, fabrication and applications*, Vol. 329 (Springer Science & Business Media, 2012).

[3] E. Mitchell, K. Hannam, J. Lazar, K. Leslie, C. Lewis, A. Grancea, S. Keenan, S. Lam, and C. Foley, "2D SQIF arrays using 20 000 YBCO high R_n Josephson junctions," Superconductor Science and Technology **29**, 06LT01 (2016).

[4] S. A. Cybart, T. Dalichaouch, S. Wu, S. Anton, J. Drisko, J. Parker, B. Harteneck, and R. Dynes, "Comparison of measurements and simulations of series-parallel incommensurate area superconducting quantum interference device arrays fabricated from $YBa_2Cu_3O_{7-\delta}$ ion damage Josephson junctions," Journal of Applied Physics **112**, 063911 (2012).

[5] S. A. Cybart, S. Wu, S. Anton, I. Siddiqi, J. Clarke, and R. Dynes, "Series array of incommensurate superconducting quantum interference devices from $YBa_2Cu_3O_{7-\delta}$ ion damage Josephson junctions," Applied Physics Letters **93**, 182502 (2008).

[6] B. Taylor, S. Berggren, M. O'Brien, B. Higa, A. L. de Escobar *et al.*, "Characterization of large two-dimensional $YBa_2Cu_3O_{7-\delta}$ SQUID arrays," Superconductor Science and Technology **29**, 084003 (2016).

[7] S. Ouanani, J. Kermorvant, D. Crété, Y. Lemaître, J. Mage, B. Marcilhac, N. Bergeal, M. Malnou, J. Lesueur, D. Mailly *et al.*, "HTS ion damage Josephson junction technology for SQUID arrays," Journal of Physics: Conference Series **507**, 042008 (2014).

[8] S. A. Cybart, E. Cho, T. Wong, V. Glyantsev, J. Huh, C. Yung, B. Moeckly, J. Beeman, E. Ulin-Avila, S. Wu *et al.*, "Large voltage modulation in magnetic field sensors from two-dimensional arrays of Y-Ba-Cu-O nano Josephson junctions," Applied Physics Letters **104**, 062601 (2014).

[9] B. L. T. Plourde and D. J. Van Harlingen, "Design of a scanning Josephson junction microscope for submicron-resolution magnetic imaging," Review of Scientific Instruments **70**, 4344 (1999).

[10] A. Shadrin, K. Constantinian, G. Ovsyannikov, S. Shitov, I. Soloviev, V. Kornev, and J. Mygind, "Fraunhofer regime of operation for superconducting quantum interference filters," Applied Physics Letters **93**, 262503 (2008).

[11] T. Golod, O. Kapran, and V. Krasnov, "Planar superconductor-ferromagnet-superconductor Josephson junctions as scanning-probe sensors," Phys. Rev. Applied **11**, 014062 (2019).

[12] A. Barone and G. Paterno, *Physics and applications of the Josephson effect* (Wiley, 1982).

[13] A. Vettoliere, C. Granata, and R. Monaco, "Long Josephson junction in ultralow-noise magnetometer configuration," IEEE Transactions on Magnetics **51**, 1 (2015).

[14] Y. M. Zhang, D. Winkler, and T. Claeson, "Detection of mm and sub-mm wave radiation from soliton and flux-flow modes in a long Josephson junction," IEEE Transactions on Applied Superconductivity **3**, 2520 (1993).

[15] V. Martin, M. L. C. Sing, D. Robbes, J. Certenais, N. Quellec, and D. Crete, "Magnetometry based on sharpened high-T_C GBJ Fraunhofer patterns," IEEE Transactions on Applied Superconductivity **7**, 3079 (1997).

[16] C. S. Owen and D. J. Scalapino, "Vortex structure and critical currents in Josephson junctions," Phys. Rev. **164**, 538 (1967).

[17] T. Yamashita, M. Kunita, and Y. Onodera, "Magnetic-field dependence of Josephson current modified by self-field," Journal of Applied Physics **39**, 5396 (1968).

[18] J. Clarke and A. B. Pippard, "Supercurrents in lead-copper-lead sandwiches," Proceedings of the Royal Society of London. Series A. Mathematical and Physical Sciences **308**, 447 (1969).

[19] J. Du, J. Lazar, S. Lam, E. Mitchell, and C. Foley, "Fabrication and characterisation of series YBCO step-edge Josephson junction arrays," Superconductor Science and Technology **27**, 095005 (2014).

[20] S. A. Cybart, S. M. Anton, S. M. Wu, J. Clarke, and R. C. Dynes, "Very large scale integration of nanopatterned $YBa_2Cu_3O_{7-\delta}$ Josephson junctions in a two-dimensional array," Nano Letters **9**, 3581 (2009).

[21] J. M. Valles, A. E. White, K. T. Short, R. C. Dynes, J. P. Garno, A. F. J. Levi, M. Anzlowar, and K. Baldwin, "Ion-beam-induced metal-insulator transition in $YBa_2Cu_3O_{7-\delta}$: A mobility edge," Phys. Rev. B **39**, 11599 (1989).

[22] N. Bergeal, J. Lesueur, M. Sirena, G. Faini, M. Aprili, J. P. Contour, and B. Leridon, "Using ion irradiation to make high-T_C Josephson junctions," Journal of Applied Physics **102**, 083903 (2007).

[23] S. A. Cybart, P. Roediger, K. Chen, J. M. Parker, E. Y. Cho, T. J. Wong, and R. C. Dynes, "Temporal stability of YBaCuO nano Josephson junctions from ion irradiation," IEEE Transactions on Applied Superconductivity **23**, 1100103 (2013).

[24] S. A. Cybart, E. Cho, T. Wong, B. H. Wehlin, M. K. Ma, C. Huynh, and R. Dynes, "Nano Josephson superconducting tunnel junctions in $YBa_2Cu_3O_{7-\delta}$ directly patterned with a focused helium ion beam," Nature Nanotechnology **10**, 598 (2015).

[25] E. Cho, M. Ma, C. Huynh, K. Pratt, D. Paulson, V. Glyantsev, R. Dynes, and S. A. Cybart, "$YBa_2Cu_3O_{7-\delta}$ superconducting quantum interference devices with metallic to insulating barriers written with a focused helium ion beam," Applied Physics Letters **106**, 252601 (2015).

[26] P. A. Rosenthal, M. Beasley, K. Char, M. Colclough, and G. Zaharchuk, "Flux focusing effects in planar thin-film grain-boundary Josephson junctions," Applied Physics Letters **59**, 3482 (1991).

[27] R. Humphreys and J. Edwards, "$YBa_2Cu_3O_7$ thin film grain boundary junctions in a perpendicular magnetic field," Physica C: Superconductivity **210**, 42 (1993).

[28] J. R. Clem, "Josephson junctions in thin and narrow rectangular superconducting strips," Physical Review B **81**, 144515 (2010).

[29] H. Kinder, P. Berberich, W. Prusseit, S. Rieder-Zecha, R. Semerad, and B. Utz, "YBCO film deposition on very large areas up to 20×20 cm^2," Physica C: Superconductivity **282-287**, 107 (1997).

[30] W. Stewart, "Current-voltage characteristics of Josephson junctions," Applied Physics Letters **12**, 277 (1968).